Ion dynamics at porous alumina surfaces

Shinnosuke Hattori,[a] Rajiv K. Kalia, Aiichiro Nakano, Ken-ichi Nomura, and Priya Vashishta
Collaboratory for Advanced Computing and Simulations, Department of Chemical Engineering and Materials Science, Department of Physics and Astronomy, and Department of Computer Science, University of Southern California, Los Angeles, California 90089-0242, USA

(Received 30 May 2012; accepted 23 July 2012; published online 7 August 2012)

Anodic porous alumina has broad applications for fabricating self-assembled nanostructures, for which atomistic understanding of ionic transport at pore surfaces is indispensable. Here, molecular-dynamics simulation of amorphous alumina with a cylindrical pore under electric field shows correlated anion (oxygen)-cation (aluminum) transport at the pore surface, as opposed to ordinary drift motion in the bulk. In particular, this phenomenon leads to "inverted" cation transport at the surface. Detailed analyses of simulation data reveal atomistic mechanisms of the correlated transport based on surface-structural relaxation and covalent oxygen-aluminum bond networks. These transport mechanisms have significant implications for alumina anodization processes. © *2012 American Institute of Physics*. [http://dx.doi.org/10.1063/1.4742869]

Anodic porous alumina[1] has broad applications in the self-assembly of nanostructures for fabricating various devices such as nanowire solar cells,[2] fuel cells,[3] energy storage,[4] and resistive random access memories.[5,6] In this technology, a regular array of cylindrical pores is formed, when aluminum is electrochemically oxidized (anodized) in certain solutions, and a thin barrier layer of alumina separates the pores from the aluminum. The fabrication technology for the anodic porous alumina has matured to the extent that the pore radius and depth are precisely controlled by the magnitude and duration of the applied electric field. In order to understand the microscopic mechanisms underlying this precise control, various theoretical and simulation studies have been performed. For example, a recent continuum simulation study shows that the viscous flow plays an important role in the formation of self-ordered anodic porous alumina structures.[7] However, the current feature size is on the order of 10-100 nm, and fabricating structures with finer features would require atomistic-level control. In particular, atomistic understanding of ionic transport at pore surfaces is indispensable for finer control of nanostructures.

Molecular dynamics (MD) simulations are ideally suited for studying atomistic dynamics underlying materials deformation, plasticity, and flow. For example, a recent MD study of amorphous silica revealed a unified underlying atomistic mechanism for these processes, i.e., motion of undercoordinated silicon and oxygen defects that migrate by switching bonds in string-like processes.[8] Alumina surfaces have been studied by MD (Refs. 9 and 10) simulations, and first principles MD simulations were performed to study the structure and dynamics of amorphous alumina.[11,12] Furthermore, MD simulations[13] along with x-ray diffraction experiments[14,15] were performed to study the structure of normal and super-cooled liquid alumina.

In this paper, we perform MD simulation to study the ionic transport under an electric field in amorphous alumina (Al_2O_3) with a cylindrical pore. The simulation results reveal surface-specific ionic transport phenomena, including enhanced oxygen transport and inverted aluminum transport at pore alumina surfaces.

Schematic of simulation setup is shown in Figs. 1(a) and 1(b). System size is $27.0\,\text{nm} \times 27.0\,\text{nm} \times 16.0\,\text{nm}$ with periodic boundary conditions in the *x*-, *y*-, and *z*-axes. Melt-quench procedure is used to prepare bulk amorphous alumina with a density of $3.0\,\text{g/cm}^3$, and subsequently atoms within a radius of 2 nm are removed to produce a cylindrical pore parallel to the *z*-axis. The interatomic potential incorporates ionic and covalent effects through a combination of two- and three-body terms.[16]

Initially, the system is heated up to 700 K, during which the radius of the pore changes to about 5 nm due to surface relaxation. After thermalization at temperature 700 K for 10 ns, an electric field of 1.0 V/nm is applied in the *z* direction.[17] The external force exerted on the *i*-th atom by the electric field **E** is

$$\mathbf{F}_i = q_i \mathbf{E}, \tag{1}$$

where q_i is the charge of the *i*-th atom taken from the interatomic potential parameters.[16]

To study the drift mobility of Al and O ions at bulk and pore-surface regions, we first divide the system into cubic cells with a side length of 0.3 nm, and compute the displacements of Al and O in each cell as

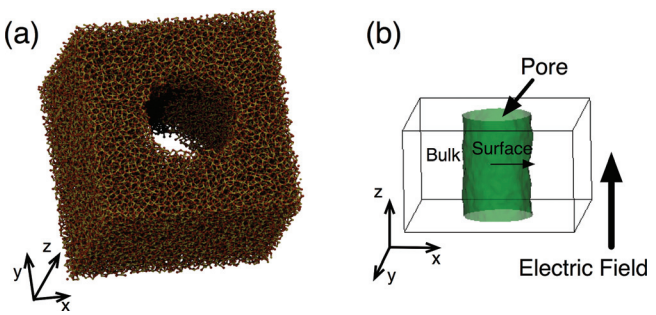

FIG. 1. (a) Snapshot of the simulated amorphous alumina structure with a cylindrical pore, where the yellow and red spheres indicate Al and O atoms, respectively. (b) Schematic of the simulated system.

[a]Also at: Sony Corporation, Atsugi-shi, Kanagawa 243-0021, Japan.

$$\Delta z_{cell}^{(\alpha)}(t) = \sum_{(i\in\alpha)\wedge(i\in cell)} (z_i(t) - z_i(t=0))/N_{cell}^{(\alpha)}, \qquad (2)$$

where α (=Al or O) is the ionic species, $z_i(t)$ is the z coordinate of the i-th atom at time t, and $N_{cell}^{(\alpha)}$ is the number of ions of species α in the cell. Figures 2(a) and 2(b), respectively, plot the calculated spatial distribution of Al and O displacements projected on the xy plane by averaging the displacements along the z-axis. The figures show distinct displacements at the pore surface from those in the bulk.

Figure 2(c) shows the averaged Al and O displacements within the pore-surface and bulk regions as a function of time, where the surface region is defined as that within 1 nm from the cylindrical pore center (see the dashed lines in Figs. 2(a) and 2(b)). In the bulk region, we observe ordinary drift mobility, i.e., Al and O move in parallel and antiparallel to the electric field, respectively. The magnitude of Al displacement is larger than that of O in the bulk. This is understandable since Al has the larger charge than O (Al^{3+} as opposed to O^{2-}), and hence the larger force exerted on it by the electric field, while its smaller ionic radius causes less steric hindrance. The most striking feature in Fig. 2(c) is the inverted Al transport at the pore surface (see the blue solid line, which shows negative displacement). Namely, Al ions on the surface drift in the opposite direction to that in the bulk. Another notable feature is that O is more mobile at the surface compared to Al. This is in contrast to the bulk region, where O is less mobile than Al (as shown in Figs. S1(a) and S1(b) in the supplementary material,[18] displacements of atoms in the radial direction have much smaller magnitudes than those in the z-direction.)

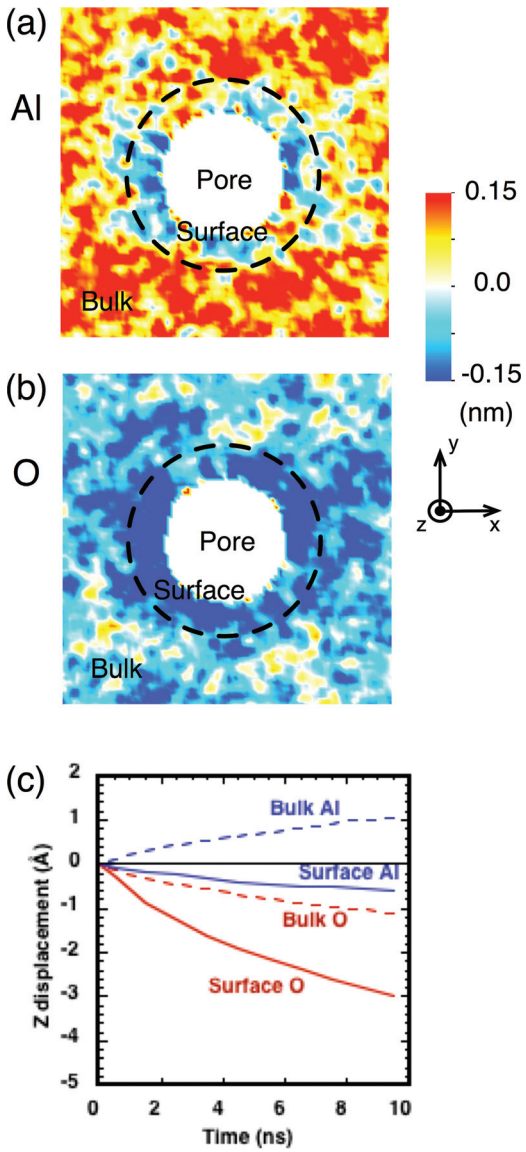

FIG. 2. Spatial distribution of atomic displacement projected on the xy plane for (a) Al and (b) O ions. Red and blue colors indicate parallel and antiparallel motions to the direction of the applied electric field, respectively. The dashed lines indicate the boundary between the surface and bulk regions. (c) Displacements of Al (blue) and O (red) ions in the z direction in the surface (solid lines) and bulk (dashed lines) regions.

To understand the mechanism underlying the unusual Al transport at the pore surface, we calculate the spatial distribution of the atomic charge and dipole moment. To do so, we again discretize the space into 1 nm cubic cells and compute the charge q_{cell} and dipole $\mathbf{d}_{cell}$ of each cell as

$$q_{cell} = \sum_{i\in cell} q_i f(r_i'), \qquad (3)$$

$$\mathbf{d}_{cell} = \sum_{i\in cell} q_i \mathbf{r}'_i f(r_i'), \qquad (4)$$

where $\mathbf{r}_i$ is the position of the i-th ion, $\mathbf{r}_{cell}$ is the center of the cell, $\mathbf{r}_i' = \mathbf{r}_i - \mathbf{r}_{cell}$, and $r_i' = |\mathbf{r}_i'|$. The charge and dipole moment of the cell are weighted averages of the contributions from individual ions using a radial weight function

$$\begin{cases} f(r) = 1 & r \le r_c \\ f(r) = \exp(-(r - r_c)/\lambda) & r > r_c \end{cases}, \qquad (5)$$

with a cutoff radius of $r_c = 1.0$ nm and a decay parameter of $\lambda = 0.3$ nm.

Figures 3(a) and 3(b) show the calculated charge and dipole-moment distributions, respectively, which are projected on the xy-plane by averaging along the z-axis. In Fig. 3(a), the color indicates the charge per unit volume, and in Fig. 3(b) the magnitude of the dipole moment is color-coded, while its magnitude and direction are, respectively, represented by the length and direction of the arrows. The charge distribution in Fig. 3(a) shows that the pore-surface region is negatively charged. Accordingly, the dipole moments at the surface in Fig. 3(b) are directed outward radially. This result is consistent with previous MD simulation,[10] in which oxygen atoms are exposed at an amorphous alumina surface to make a negatively charged surface. Also, previous quantum-mechanical (QM) calculations show considerable surface relaxation on Al_2O_3 (0001) surface, where the surface O atoms are displaced outward relative to surface Al atoms.[19,20]

We also calculate the radial profile of the stoichiometry by averaging the local charge in a concentric shell of thickness 1.0 nm around the center of the pore. The result in Fig. 4 reveals an oxygen-rich stoichiometry, O/Al $\sim$ 3 at the surface, as compared to the bulk value of 3/2, reflecting the negative charged pore surface. This result is consistent with magic-angle-spinning (MAS) and multiple-quantum magic-angle-spinning (MQMAS) nuclear magnetic resonance (NMR) experiments,[21] which indicate that the surface layers and the bulk of porous

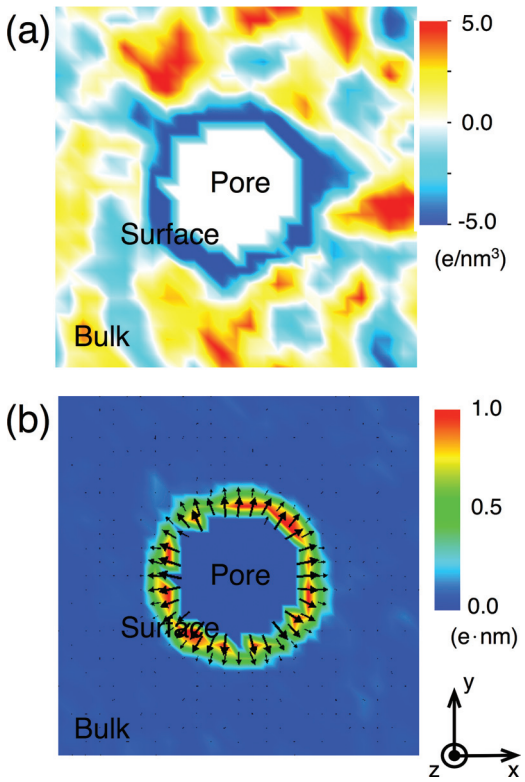

FIG. 3. Spatial distribution of the charge (a) and dipole moment (b) projected on the *xy* plane.

alumina are composed of [AlO_6] and [AlO_4 and AlO_5], respectively. Namely, the pore surface is more oxygen rich compared to the bulk.

In network glasses such as alumina and silica, cations and anions are covalently bonded, and ionic transport is dictated by their correlated motions.[8] At the negatively charged pore surface, the majority ionic current carrier (O) tends to drag the minority carrier (Al) with them, resulting in Al motion that is opposite to the bulk Al motion. This in turn generates a shear Al flow between the surface and bulk. The velocity field in Fig. S2 in the supplementary material[18] shows the resulting complex flow pattern near a pore surface.

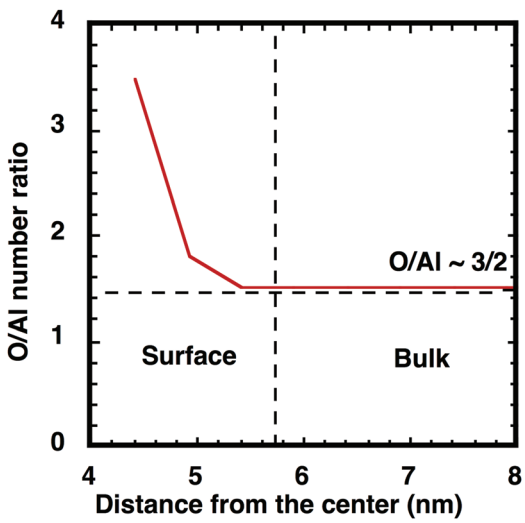

FIG. 4. Local stoichiometry (i.e., the ratio between the numbers of O and Al atoms) as a function of the distance from the cylindrical center.

Such a complex flow pattern arising from cation-anion correlation is not considered in continuum simulations of viscous flow during the formation of self-ordered anodic porous alumina structures.[7] Similar atomistic correlation effects may provide refined constitutive relations and nontrivial boundary conditions to such continuum simulations.

In QM (Refs. 19 and 20) and variable-charge MD (Refs. 22 and 23) simulations, Al and O atoms at alumina surfaces are shown to have slightly smaller magnitudes of charge. To examine how the reduced surface atomic charges modify the results obtained by the fixed-charge MD method described above, we have performed another set of simulations using the reactive force field (ReaxFF),[24] which incorporates variable charges depending on the local stoichiometry based on the electronegativity equalization approach.[25] Figure S3 in the supplementary material[18] compares the spatial distribution of charge and dipole moment calculated by the MD and ReaxFF-MD methods. Although with a reduced magnitude, the ReaxFF-MD result still exhibits negative charges at the pore surface as in the MD case. Figure S4 plots the spatial distribution of Al and O displacements projected on the *xy* plane by averaging the displacements along the *z*-axis. The ReaxFF-MD result exhibits the inverted Al motion as in the MD result in Fig. 2. Namely, the surface-specific ionic motions found in our MD simulation are not likely artifacts of the interatomic potential.

In summary, our MD simulation has revealed a surface-specific ionic transport phenomenon under an electric field at an anodic porous alumina surface. It is caused by the stoichiometry difference that exposes a negatively charged surface. This phenomenon may play an important role in nanoionics-based porous alumina growth mechanisms to control self-assembly processes.

This work was supported by DOE-BES (Grant No. DE-FG02-04ER46130).

[1]H. Masuda and K. Fukuda, Science **268**(5216), 1466–1468 (1995).
[2]D. D. Li, L. A. Zhao, C. H. Jiang, and J. G. Lu, Nano Lett. **10**(8), 2766–2771 (2010).
[3]J. C. Ganley, E. G. Seebauer, and R. I. Masel, AIChE J. **50**(4), 829–834 (2004).
[4]P. Banerjee, I. Perez, L. Henn-Lecordier, S. B. Lee, and G. W. Rubloff, Nat. Nanotechnol. **4**(5), 292–296 (2009).
[5]S.-H. Lyu and J.-S. Lee, J. Mater. Chem. **22**(5), 1852–1861 (2012).
[6]J. Lee, S. Nigo, Y. Nakano, S. Kato, H. Kitazawa, and G. Kido, Sci. Technol. Adv. Mater. **11**(2), 025002 (2010).
[7]J. E. Houser and K. R. Hebert, Nat. Mater. **8**(5), 415–420 (2009).
[8]K. I. Nomura, Y. C. Chen, R. K. Kalia, A. Nakano, and P. Vashishta, Appl. Phys. Lett. **99**(11), 111906 (2011).
[9]S. Blonski and S. H. Garofalini, Surf. Sci. **295**(1–2), 263–274 (1993).
[10]S. P. Adiga, P. Zapol, and L. A. Curtiss, Phys. Rev. B **74**(6), 064204 (2006).
[11]G. Gutierrez, A. Taga, and B. Johansson, Phys. Rev. B **65**(1), 012101 (2001).
[12]S. Davis and G. Gutierrez, J. Phys.: Condens. Matter **23**(49), 495401 (2011).
[13]G. Gutierrez, A. B. Belonoshko, R. Ahuja, and B. Johansson, Phys. Rev. E **61**(3), 2723–2729 (2000).
[14]S. Ansell, S. Krishnan, J. K. R. Weber, J. J. Felten, P. C. Nordine, M. A. Beno, D. L. Price, and M. L. Saboungi, Phys. Rev. Lett. **78**(3), 464–466 (1997).
[15]S. Krishnan, L. Hennet, S. Jahn, T. A. Key, P. A. Madden, M. L. Saboungi, and D. L. Price, Chem. Mater. **17**(10), 2662–2666 (2005).
[16]P. Vashishta, R. K. Kalia, A. Nakano, and J. P. Rino, J. Appl. Phys. **103**(8), 083504 (2008).
[17]We adopt a typical experiment growth voltage, but at an appropriate temperature for observing ionic transport within the simulated timespan.

[18]See supplementary material at http://dx.doi.org/10.1063/1.4742869 for simulation details.
[19]I. Manassidis, A. Devita, and M. J. Gillan, Surf. Sci. **285**(3), L517–L521 (1993).
[20]X. G. Wang, A. Chaka, and M. Scheffler, Phys. Rev. Lett. **84**(16), 3650–3653 (2000).
[21]T. Iijima, S. Kato, R. Ikeda, S. Ohki, and G. Kido, Chem. Lett. **34**(9), 1286–1287 (2005).
[22]F. H. Streitz and J. W. Mintmire, Phys. Rev. B **50**(16), 11996–12003 (1994).
[23]T. J. Campbell, R. K. Kalia, A. Nakano, P. Vashishta, S. Ogata, and S. Rodgers, Phys. Rev. Lett. **82**(24), 4866–4869 (1999).
[24]Q. Zhang, T. Cagin, A. van Duin, W. A. Goddard, Y. Qi, and L. G. Hector, Phys. Rev. B **69**(4), 045423 (2004).
[25]A. K. Rappe and W. A. Goddard, J. Phys. Chem. **95**(8), 3358–3363 (1991).